Transient eddies in the southern hemisphere of Mars

D. P. Hinson
Department of Electrical Engineering, Stanford University, Stanford, California, USA

R. J. Wilson
Geophysical Fluid Dynamics Laboratory/NOAA, Princeton University, Princeton, New Jersey, USA

Received 18 September 2001; revised 4 December 2001; accepted 5 December 2001; published 13 April 2002.

[1] Mars Global Surveyor is providing the first observations of transient eddies in the southern hemisphere of Mars. We derive basic properties of the traveling eddies that appear in midwinter (L_s = 134°–148°) through analysis of radio occultation measurements at 67°–70°S latitude. The dominant mode has a period of ~2 solar days and a zonal wavenumber s = 3. Strong zonal variations in eddy amplitude signal the presence of a possible "storm zone" at 150°–330°E longitude. Within this longitude band the eddies achieve peak amplitudes at the 300-Pa pressure level of ~7 K in temperature and 10–15 m s^{-1} in meridional wind speed. The minimum temperature associated with the eddies is ~2 K colder than saturation of CO_2, close to the threshold where nucleation and growth of new ice particles can occur. A simulation by a Mars general circulation model produces traveling eddies that closely resemble the observations. *INDEX TERMS:* 5409 Planetology: Solid Surface Planets: Atmospheres—structure and dynamics; 3346 Meteorology and Atmospheric Dynamics: Planetary meteorology (5445, 5739); 5445 Planetology: Solid Surface Planets: Meteorology (3346); 6225 Planetology: Solar System Objects: Mars

1. Introduction

[2] Planetary scale transient eddies (or weather systems) have been observed in the northern hemisphere of Mars by the Viking Landers [*Ryan et al.*, 1978; *Barnes*, 1980, 1981] and possibly by the infrared sounder on Mariner 9 [*Conrath*, 1981]. The Lander measurements span several Martian years, allowing studies of seasonal and interannual variability [*Leovy et al.*, 1985; *Zurek et al.*, 1992] and providing a foundation for numerical simulations with Martian general circulation models (MGCMs) [*Barnes et al.*, 1993; *Collins et al.*, 1996]. In the absence of analogous observations in the southern hemisphere, our understanding of transient eddies in that region has remained speculative.

[3] This paper reports the first observations of transient eddies in the southern hemisphere of Mars. (We will also refer to these disturbances as traveling waves, although their precise nature is uncertain.) We derive basic characteristics of the traveling wave modes through analysis of radio occultation data obtained with Mars Global Surveyor (MGS). We also explore the winter dynamics of the southern hemisphere through use of the MGCM of the NOAA Geophysical Fluid Dynamics Laboratory [*Wilson and Hamilton*, 1996]. By comparing the measured eddies with simulations we gain deeper insight into their behavior as well as important validation of the MGCM.

[4] Figure 1 shows the mean temperature and zonal wind fields as simulated by the MGCM, which provide a context for the observations. The season is midwinter of the southern hemisphere (L_s = 145°). The simulated thermal structure compares favorably with measurements at this season by the MGS Thermal Emission Spectrometer [*Smith et al.*, 2001]. The model wind field includes not only a baroclinic component in thermal wind balance with the temperature field but also a barotropic component, which can be significant, particularly within the lowest scale height. The presence in the southern hemisphere of a strong south-to-north temperature gradient and a pronounced eastward jet in the zonal winds suggests the possibility of baroclinic and/or barotropic instability, which can initiate and sustain transient eddies.

0094-8276/02/2001GL014103$05.00

2. Observations

[5] The Sun-synchronous, polar orbit of MGS provides frequent opportunities for radio occultation sounding of the neutral atmosphere, which is conducted routinely as part of the Radio Science (RS) investigation [*Tyler et al.*, 2001]. The basic result of each observation is a profile of pressure and temperature versus planetocentric radius and geopotential [*Hinson et al.*, 1999]. More than 4000 profiles were obtained during the 687-day mapping phase of the mission, and additional observations are underway.

[6] Of interest here is a set of 267 RS profiles at 67°–70°S latitude for L_s = 134°–148° (May 1999). The Sun was ~5° above the horizon at the local time of these observations (~1040). The separation in longitude between successive profiles is 28.6°, providing daily sampling of zonal structure through wave number 6. As a given longitude is sampled only once per day, traveling waves with a period of 2 days or less are subject to aliasing.

[7] Both transient eddies and stationary planetary waves appear in these measurements. For example, Figure 2a shows samples of temperature versus longitude at 300 Pa. The solid line shows the stationary component of the temperature field obtained by fitting zonal harmonics through wave number 4 to all data within this 25-day interval. (The method of analysis is described elsewhere [*Hinson et al.*, 2001].) At this pressure the spectrum of stationary waves is dominated by the wave-1 and wave-2 components, each with an amplitude of ~1 K. The data samples are clustered about this zonal trend except at longitudes of 150°–330°E, where prominent outliers signal the presence of transient waves.

[8] Figure 2b illustrates the zonal and temporal structure of the waves. Measurements are shown from 4 consecutive days for L_s = 144.6°–146.6°, an interval that contains several siginficant outliers. The heavy and light solid lines show results on the first and third days in the sequence, while results on the second and fourth days are depicted by heavy and light dashed lines. Measurements on successive days are ~180° out of phase at longitudes of 150°–330°E, where day-to-day temperature variations are as large as 15 K. Within each day, the maximum and minimum temperatures are separated by ~60° in longitude.

[9] We characterized the traveling eddies within this 4-day interval through least squares analysis, solving for the period P and zonal wavenumber s (an integer). It is not possible to determine the direction of travel due to aliasing. There is a pair of solutions with $P \approx 2$ days, one traveling eastward with s = 3 and

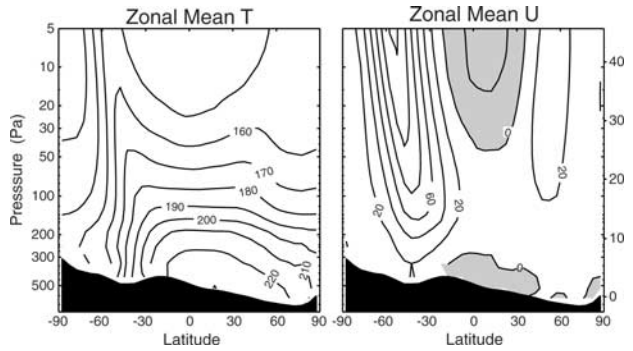

Figure 1. MGCM simulation of (left) temperature and (right) zonal winds for L_s = 145°. Both fields have been averaged over time and longitude. Contour intervals are 10 K and 20 m s^{-1}, respectively. Shading denotes negative (westward) winds. The vertical axes show (left) pressure in Pa and (right) approximate altitude in km.

the other traveling westward with s = 4. Additional solutions with $P \approx 2/3$ or 2/5 days are mathematically possible. Two considerations help resolve this ambiguity. First, the baroclinic waves observed in the northern hemisphere by the Viking landers have periods of 2–10 days [*Barnes et al.*, 1993; *Collins et al*, 1996].

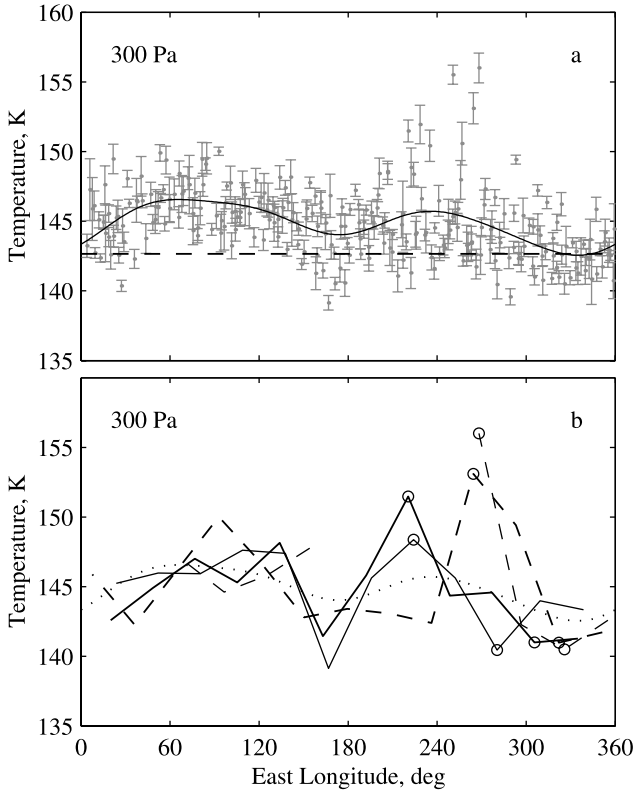

Figure 2. (a) Temperature at 300 Pa from RS profiles at 67°–70°S, L_s = 134°–148°. Error bars correspond to one standard deviation. The solid line is a least squares solution for zonal variations due to stationary planetary waves, which also appears as a dotted line in the lower panel. The dashed line shows the saturation temperature of CO_2. (b) Subset of data from the upper panel. Measurements on 4 consecutive days are shown by heavy solid, heavy dashed, light solid, and light dashed lines, respectively.

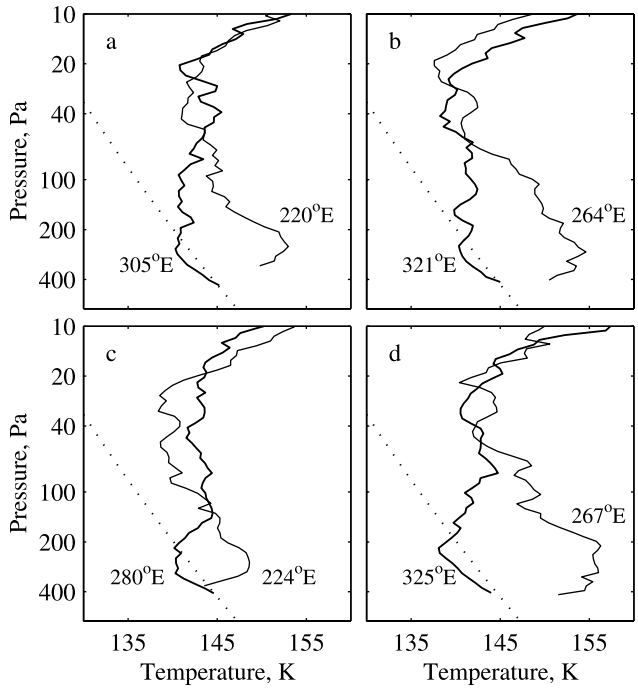

Figure 3. Selected RS temperature profiles at 67°S for L_s = 144.6°–146.6°. One pair of profiles is shown from each day of the sequence in Figure 2b. Samples in Figure 2b corresponding to these profiles are labeled with a circle. The dotted line in each panel shows the saturation temperature of CO_2.

Only the "long" period solutions fall within this range. Second, simple models for baroclinic instability predict that the wave phase speed should match the mean zonal wind speed at the "steering level" [*Gill*, 1982]. For the zonal mean circulation in Figure 1, disturbances would therefore be expected to travel eastward at mid-to-high southern latitudes where eastward winds predominate. Hence the data in Figure 2b most likely reflect the presence of a wave traveling eastward with $P \approx 2$ days, s = 3, and a zonal phase speed of 15 m s^{-1}.

[10] We examined other subsets of the data in Figure 2a in this manner. Traveling disturbances appear intermittently at intervals of 5–7 days, producing prominent temperature deviations at longitudes of 150°–330°E that persist for a few days. The period and zonal wave number of these eddies are consistent with the values given above. During the intervening quiescent periods, temperatures rarely deviate by more than 2 K from the zonal trend.

[11] Figure 3 shows the vertical structure of the eddies. Each panel contains a pair of profiles from 1 day of the 4-day sequence in Figure 2b. The profiles were selected within each day to illustrate the warmest and coldest phases of the disturbance, which are separated by ~60° in longitude. Each profile extends to within a few hundred meters of the surface. The wave amplitude is appreciable at pressures exceeding ~50 Pa, corresponding to altitudes below ~16 km, with a peak amplitude of ~7 K at 200–300 Pa. The peak amplitude in geopotential height (not shown) is ~200 m; for quasi-geostrophic flow the corresponding meridional winds have an amplitude of 10–15 m s^{-1}.

3. MGCM Simulation

[12] The MGCM results shown here, including those in Figure 1, are based on a version of the model with a horizontal resolution of 5° in latitude by 6° in longitude and 40 vertical layers extending from the surface to ~90 km altitude. The simulation includes injection of radiatively active dust into the atmosphere by dust

devils. The spatial distribution of dust is coupled to the evolving atmospheric circulation, yielding a zonal mean dust distribution that decreases markedly from equator to pole [*Wilson*, 2000].

[13] Traveling waves appear in the MGCM simulation in the region sampled by the RS experiments. As an illustration of their general behavior, Plate 1 shows the variations of meridional wind speed at 300 Pa and 67.5°S. This longitude-time plot contains a distinct pattern of waves traveling eastward with the same basic properties as the observed waves: $P \approx 2$ days, $s = 3$, with a peak amplitude of ~15 m s^{-1}. However, these simulated waves persist through most of the 17-day interval in Plate 1, and in this respect their behavior differs from the more intermittent observed waves.

[14] Plate 2 shows the simulated temperature and horizontal wind fields of the traveling eddies at a selected time. Contributions from stationary waves and thermal tides have been removed with a band-pass filter. In both Plates 1 and 2 the eddy amplitude is zonally modulated so that the strongest eddies appear at longitudes of 180°–330°E. Temperature variations within this longitude band have an amplitude of ~10 K. Encouraged by these similarities between the simulated and measured eddies, we are currently using the MGCM to gain a deeper understanding of their behavior.

4. Discussion

[15] In both the RS measurements in Figure 2 and the MGCM simulation in Plates 1 and 2, the eddy amplitude varies strongly with longitude. MGCM simulations of baroclinic waves in the northern hemisphere also exhibit this type of behavior, with "storm zones" of enhanced wave activity appearing within the low lying planitia [*Hollingsworth et al.*, 1996]. The southern storm zone has no obvious association with surface topography, and its origin is currently under investigation.

[16] For CO_2 the relation between saturation vapor pressure p_s (in Pa) and temperature T (in K) takes the form [*James et al.*, 1992]

$$\ln p_s = 29.8246 - 3311.57T^{-1} - 6.71 \times 10^{-3}T \qquad (1)$$

for 100 K < T < 170 K. This equation can be inverted to obtain the saturation temperature T_s for a given partial pressure. Figure 3 shows T_s as a function of the total atmospheric pressure, which exceeds the CO_2 partial pressure by ~5%.

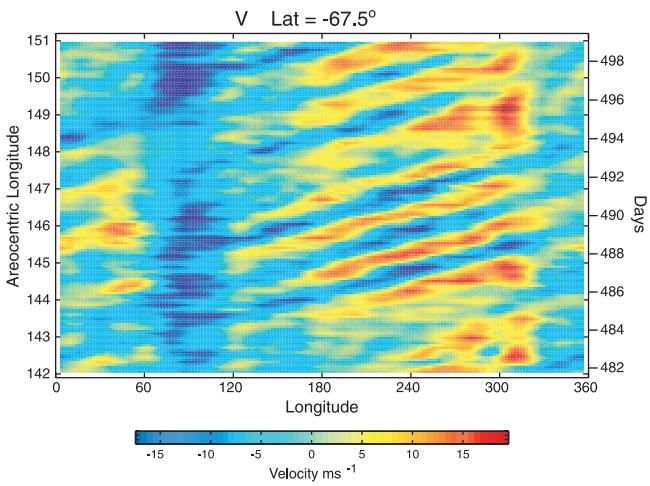

Plate 1. Meridional winds (in m s^{-1}) at 300 Pa and 67.5°S as simulated by the MGCM. The time scale is labeled at left in L_s and at right in solar days. Positive winds are equatorward. Waves traveling eastward appear as patterns sloping from lower left to upper right. Stationary waves are also present, producing steady poleward winds near 90°E.

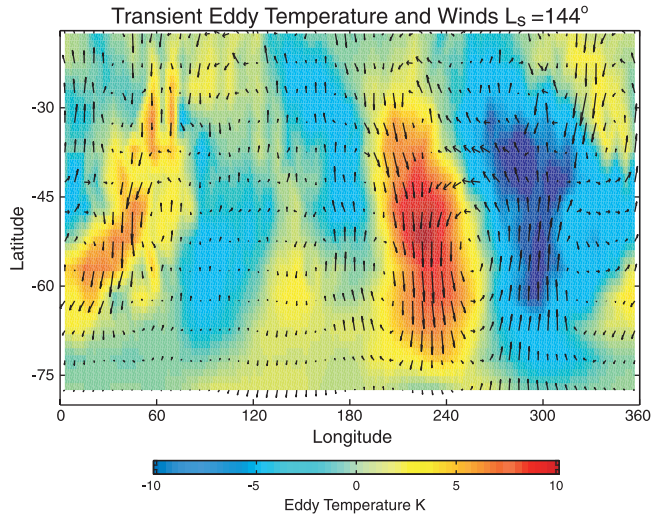

Plate 2. Synoptic map of the temperature and horizontal wind fields of the traveling eddies in the MGCM simulation. Results are shown at the 300-Pa pressure level for L_s = 144°. Temperatures (in K) are indicated by color shading. Wind speed and direction are indicated by the length and orientation of the arrows. Warm temperatures are closely aligned with poleward flow and cool temperatures with equatorward flow.

[17] In each panel of Figure 3 one of the measured profiles is colder than the saturation profile at pressures of 200–400 Pa. The difference is as large as ~2 K. These cold regions are clearly associated with equatorward advection of cold air by the traveling waves, but supersaturation requires additional thermal forcing, possibly due to adiabatic ascent. Figure 2a shows that supersaturation occurs most frequently at longitudes of ~170°E and ~330°E, near the temperature minima of the stationary waves.

[18] Recent laboratory measurements have shown that heterogeneous nucleation of CO_2 does not occur until its partial pressure exceeds p_s by ~35% [*Glandorf et al.*, 2002; *Colaprete and Toon*, 2002]. This corresponds to a temperature ~2 K less than T_s. Hence the "cold" profiles in Figure 3 are near the threshold where nucleation and growth of new CO_2 ice particles can occur. Note that the temperature approaches saturation at the base of these profiles, where the presence of seasonal CO_2 ice at the surface prevents supersaturation.

[19] **Acknowledgments.** Funding for this work was provided by the MGS Project and the NASA Mars Data Analysis Program.

References

Barnes, J. R., Time spectral analysis of midlatitude disturbances in the Martian atmosphere, *J. Atmos. Sci.*, *37*, 2002–2015, 1980.

Barnes, J. R., Midlatitude disturbances in the Martian atmosphere: A second Mars year, *J. Atmos. Sci.*, *38*, 225–234, 1981.

Barnes, J. R., J. B. Pollack, R. M. Haberle, C. B. Leovy, R. W. Zurek, H. Lee, and J. Schaeffer, Mars atmospheric dynamics as simulated by the NASA Ames general circulation model, 2, Transient baroclinic eddies, *J. Geophys. Res.*, *98*, 3125–3148, 1993.

Colaprete, A., and O. B. Toon, Carbon dioxide clouds at high altitude in the tropics and in an early dense Martian atmosphere, *Icarus*, in press, 2002.

Collins, M., S. R. Lewis, P. L. Read, and F. Hourdin, Baroclinic wave transitions in the Martian atmosphere, *Icarus*, *120*, 344–357, 1996.

Conrath, B. J., Planetary-scale wave structure in the Martian atmosphere, *Icarus*, *48*, 246–255, 1981.

Gill, A. E., *Atmosphere-Ocean Dynamics*, 662 pp., Academic, San Diego, Calif., 1982.

Glandorf, D. L., T. Colaprete, M. A. Tolbert, and O. B. Toon, CO_2 snow on Mars and early Earth: Experimental constraints, *Icarus*, in press, 2002.

Hinson, D. P., R. A. Simpson, J. D. Twicken, G. L. Tyler, and F. M. Flasar, Initial results from radio occultation measurements with Mars Global Surveyor, *J. Geophys. Res.*, *104*, 26,997–27,012, 1999.

Hinson, D. P., G. L. Tyler, J. L. Hollingsworth, and R. J. Wilson, Radio occultation measurements of forced atmospheric waves on Mars, *J. Geophys. Res.*, *106*, 1463–1480, 2001.

Hollingsworth, J. L., R. M. Haberle, J. R. Barnes, A. F. C. Bridger, J. B. Pollack, H. Lee, and J. Schaeffer, Orographic control of storm zones on Mars, *Nature*, *380*, 413–416, 1996.

James, P. B., H. H. Kieffer, and D. A. Paige, The seasonal cycle of carbon dioxide on Mars, in *Mars*, edited by H. H. Kieffer, et al., pp. 934–968, Univ. of Ariz. Press, Tucson, 1992.

Leovy, C. B., J. E. Tillman, W. R. Guest, and J. Barnes, Interannual variability of Martian weather, in *Recent Advances in Planetary Meteorology*, edited by G. E. Hunt, pp. 69–84, Cambridge Univ. Press, New York, 1985.

Ryan, J. A., R. M. Henry, S. L. Hess, C. B. Leovy, J. E. Tillman, and C. Walcek, Mars meteorology: Three seasons at the surface, *Geophys. Res. Lett.*, *5*, 715–718, 1978.

Smith, M. D., J. C. Pearl, B. J. Conrath, and P. R. Christensen, Thermal Emission Spectrometer results: Mars atmospheric thermal structure and aerosol distribution, *J. Geophys. Res.*, *106*, 23,929–23,945, 2001.

Tyler, G. L., et al., Radio Science observations with Mars Global Surveyor: Orbit insertion through one year in mapping, *J. Geophys. Res.*, *106*, 23,327–23,348, 2001.

Wilson, R. J., and K. Hamilton, Comprehensive model simulation of thermal tides in the Martian atmosphere, *J. Atmos. Sci.*, *53*, 1290–1326, 1996.

Wilson, R. J., Evidence for diurnal period Kelvin waves in the Martian atmosphere from Mars Global Surveyor TES data, *Geophys. Res. Lett.*, *27*, 3889–3892, 2000.

Zurek, R. W., J. R. Barnes, R. M. Haberle, J. B. Pollack, J. E. Tillman, and C. B. Leovy, Dynamics of the atmosphere of Mars, in *Mars*, edited by H. H. Kieffer, et al., pp. 835–933, Univ. of Ariz. Press, Tucson, 1992.

D. P. Hinson, Department of Electrical Engineering, Stanford University, 350 Serra Mall, Stanford, CA 94305-9515, USA. (hinson@nimbus.stanford.edu)

R. J. Wilson, Geophysical Fluid Dynamics Laboratory (NOAA), Princeton University Forrestal Campus, P.O. Box 308, Princeton, NJ 08542, USA. (rjw@gfdl.noaa.gov)